Chinese Chemical Letters 36 (2025) 110375

Contents lists available at ScienceDirect

Chinese Chemical Letters

journal homepage: www.elsevier.com/locate/cclet

Ultralong room temperature phosphorescence and broad color-tunability persistent luminescence *via* new strategy

Hong Yao*, Feixiang Yang, Jianpeng Hu, Wenyu Cao, Shuning Qin, Tai-Bao Wei, Bingbing Shi, Qi Lin*

Key Laboratory of Eco-Functional Polymer Materials of the Ministry of Education, Key Laboratory of Polymer Materials of Gansu Province, College of Chemistry and Chemical Engineering, Northwest Normal University, Lanzhou 730070, China

ARTICLE INFO

Article history:
Received 30 May 2024
Revised 17 August 2024
Accepted 26 August 2024
Available online 27 August 2024

Keywords:
Polyatomic synergistic effect
RTP
PRET
Multilevel anti-counterfeiting
Underwater phosphorescence

ABSTRACT

Pure organic materials with ultralong room-temperature phosphorescence (RTP) and persistent luminescence in broad color gamut exhibit tremendous potential and broad application prospects due to their unique optical properties. This article proposes a simple strategy, polyatomic synergistic effect, to endow persistent luminescent materials with ultralong lifetime and broad color-tunability through polyatomic synergistic effect and non-traditional phosphorescence resonance energy transfer (PRET). By leveraging the polyatomic synergistic effect to enhance the intersystem crossing (ISC) in bibenzimidazole (BBI) derivatives and suppress the non-radiative transition process, ultralong persistent room-temperature phosphorescence has been successfully achieved after incorporating BBI-Cl-M into poly(methyl methacrylate) (PMMA) to form a rigid matrix(BBI-Cl-M@PMMA). Specifically, the ester functionalized bibenzimidazole with modified chlorine on molecular skeleton (BBI-Cl-M) demonstrates a remarkable phosphorescent lifetime (τ_p) of up to 256.4 ms. In addition, the behaviors and mechanism of RTP *via* polyatomic synergistic effect have been further understood by theoretical calculation and single crystal analysis. Subsequently, utilizing BBI-Cl-M as the energy donor and Rhodamine B (RB) as the energy acceptor, persistent and multicolor organic afterglow covering from green to red has been realized successfully by simply regulating the doping composition and concentration of PRET systems. These RTP materials have also been applied in underwater afterglow emission and multilevel anti-counterfeiting technology successfully.

Ultralong organic room temperature phosphorescence (UORTP) materials, owning individual long-lasting triplet excitons and significant Stokes shift, is captivating for their diverse nature, such as affordability, low toxicity, tunable optical properties and responsiveness to stimuli [1-4], which benifit UORTP to be applied potentially in bioimaging [5], advanced encryption, anti-counterfeiting [6-9] and high-sensitivity sensors [10-12]. The design and fabrication of UORTP materials with excellent performance have emerged as a leading area over the past few years [13-20]. However, the spin-forbidden intersystem crossing (ISC) process from singlet to triplet states and the weak spin-orbit coupling (SOC) pose significant challenges for organic luminophores to demonstrate RTP. Up to now, a variety of strategies have been put forward to improve the RTP properties of pure organic systems. For example, the introduction of carbonyl groups [21], heteroatoms [22] and halogen atoms [23] can raise spin–orbit coupling (SOC) to generate triplet excitons. Meanwhile, strategies such as utilizing crystallization engineering [24,25], incorporating organic phosphorescent materials into solid polymeric matrix [26,27] or supramolecular host cavity [28] and constructing H-aggregation [29] or 3D networks [30] can be capable of reducing non-radiative transitions channels obviously [31-35]. Despite of above significant advancements, developing new strategies to achieve UORTP remains challenging.

Materials with broad multi-color luminescent properties have a critical function in the realm of anti-counterfeiting technology. Therefore, the development of materials that not only have an ultralong lifetime but also offer a broad range of color adjustments in continuous luminescence is of great significance for realizing multi-level anti-counterfeiting. Accordingly, a range of attempts have been done to achieve this target [36], principally consisting of the investigation of novel chromophores, the assembly of diverse clusters and aggregates, the incorporation of minor ingredients, the covalent connection of multiple chromophores and the implementation of phosphorescence resonance energy transfer (PRET). Among these approaches, the PRET strategy stands out for its distinct benefit of eliminating the need for intricate molecular design and synthesis processes. The process of PRET is de-

* Corresponding authors.
E-mail addresses: yhxbz@126.com (H. Yao), linqi2004@126.com (Q. Lin).

https://doi.org/10.1016/j.cclet.2024.110375
1001-8417/

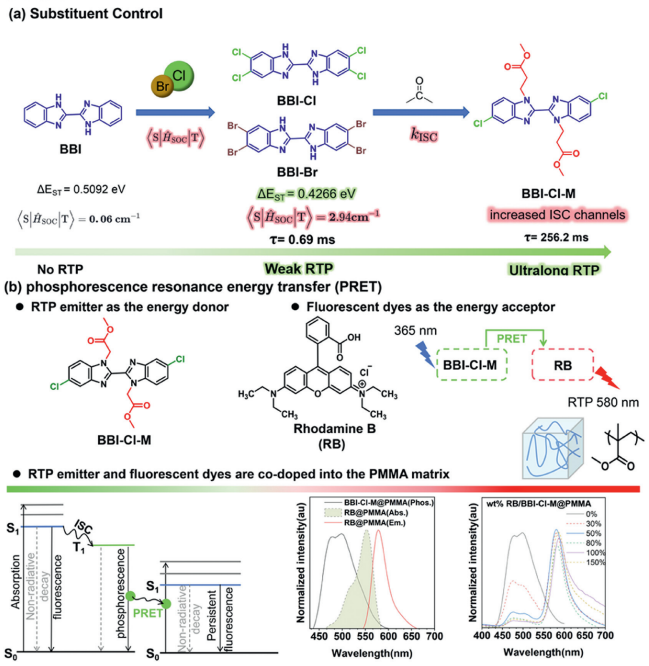

Fig. 1. (a) Chemical structures of energy donors (organic RTP emitters). (b) Depiction of the processes involved in PRET.

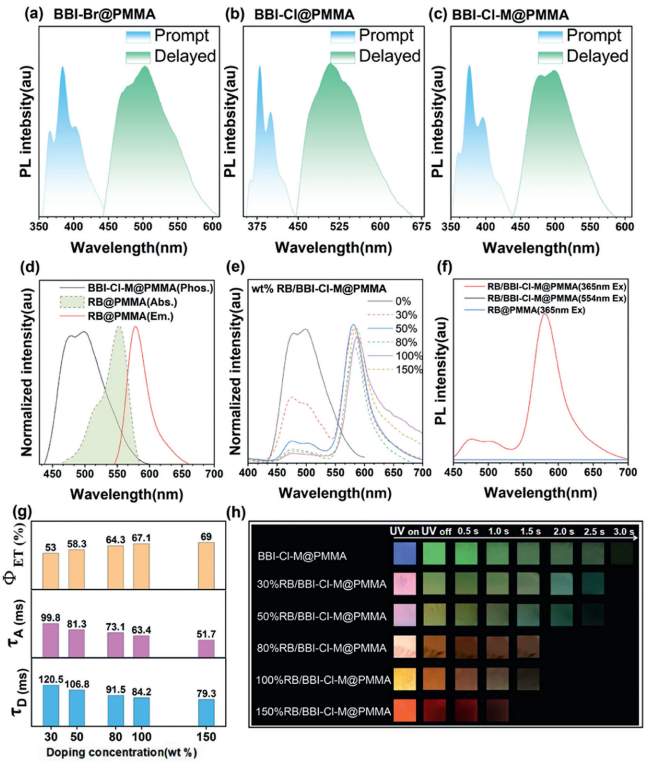

Fig. 2. (a-c) Optical characteristics of doped PMMA films BBI-Br@PMMA, BBI-Cl@PMMA and BBI-Cl-M@PMMA (Instantaneous and delayed photoluminescence spectra). Optical characteristics of co-doped PMMA film with RB/BBI-Cl-M@PMMA: (d) Combined absorption, fluorescence and phosphorescence spectra. (e) Variation in prompt and delayed emission spectra with the concentration of RB. (f) Alterations in delayed emission spectra based on the excitation wavelength. (g) Data chart for the photophysical parameters of the PRET process. (h) Images of the luminescence during and subsequent to the cessation of UV light exposure (365 nm) for various time intervals.

pendent on the proximity of the donor and acceptor, involving the transfer of energy from the donor's excited triplet state to the acceptor's excited singlet state, which then leads to the acceptor releasing fluorescence over an extended period. In comparison with common fluorescence resonance energy transfer (FRET), PRET is capable of not only modulating the color of the organic afterglow but also significantly enhancing the fluorescence lifetime by multiple orders of magnitude. For example, PRET have been introduced to achieve adjustable and even near-infrared (NIR) afterglow by controlling the dopant compositions and concentrations [37-41]. Thus far, organic afterglow systems featuring color tunability, stimulus sensitivity and NIR emission have been constructed by co-assembly of energy donor and acceptor units within a polymeric rigid framework [35,37,42-45]. Although substantial progress has been made, organic afterglow materials that possess the combined characteristics of ultralong-lasting emission, adaptable color and phosphorescence-fluorescence linkage luminescence are seldom documented.

In this work, a simple strategy to endow luminescent materials the qualities of an ultralong lifetime and broad color-tunability by polyatomic synergistic effect in conjunction with non-traditional PRET was proposed. Firstly, the design of BBI-Cl-M@PMMA takes into account the following factors: (i) The synergistic action of multiple atoms can promote intersystem crossing (ISC) while suppressing non-radiative transition processes simultaneously, (ii) the polymethyl methacrylate (PMMA) matrix can further enhance the rigidity of the material and suppress the occurrence of non-radiative transitions. After doping BBI-Cl-M into the PMMA matrix, it exhibits UORTP characteristics as expected, with a lifetime reaching up to 265.2 ms. Consequently, BBI-Cl-M as selected triplet energy donor, paired with RB as the energy acceptor, has demonstrated exceptional PRET performance (Fig. 1). By the PRET mechanism, an impressive persistent red emission with a lifetime of 99.8 ms has been achieved. Moreover, RTP emission of the composite materials spans a broad wavelength range from green to red, realizing multicolored luminescence effect. Excitingly, its underwater phosphorescent performance such as intensity and lifetime, both surpasses that in air, owning to the embedment effect of the PMMA film. Furthermore, we have explored various encryption patterns to showcase the potential of bibenzimidazole derivatives in multilevel anti-counterfeiting. The BBI-Cl-M@PMMA film, with its unique UORTP characteristics, has also been successfully applied in underwater model making. All of above offer new possibilities for future applications in complex environments, such as underwater phosphorescence, security marking, information encryption and bioimaging.

Initially, halogen atoms were introduced on both sides of the bibenzimidazole skeleton. Given the existence of multiple isomers for the monohalogenation of the benzimidazole group, we opted to introduce halogen atoms both at the 5 and 6 positions of each benzimidazole (BBI-Cl and BBI-Br). Upon doping these derivatives into the PMMA matrix and irradiating with a 365 nm UV lamp, a brief green afterglow was observed. Specifically, the afterglow time for BBI-Br was close to 0 s with a phosphorescence lifetime of 0.69 ms, whereas for BBI-Cl, the afterglow time approached 1 s with a phosphorescence lifetime of 160.2 ms (Figs. 2a-c and Fig. S19 in Supporting information). These results indicate that the introduction of halogen atoms offers the possibility of achieving room-temperature phosphorescence in BBI derivatives. To achieve a longer phosphorescence lifetime (τ_p), we are wondering photophysical properties through polyatomic synergistic effect. Subsequently, through a one-step substitution reaction, ester whether other kinds of atom could be introduced into the same molecular skeleton to alter molecular orbitals and further affect groups were introduced into the bibenzimidazole skeleton, incorporating a chlorine atom and ester groups (BBI-Cl-M). Upon incorporation of these derivatives into the PMMA matrix, a luminous green afterglow with a duration of 3 s

was noted, accompanied by a marked extension of the phosphorescence lifetimes to 256.2 ms (Figs. S16 and S19 in Supporting information). In BBI derivatives where only ester groups were introduced without the presence of chlorine atoms, room-temperature phosphorescence was not observed. Thus, the simultaneous promotion effect of halogen atoms and ester groups, polyatomic synergistic effect may be a crucial factor in achieving ultralong RTP in BBI derivatives (Fig. 1).

Given that BBI-Cl-M@PMMA demonstrates ultralong RTP within the spectral range of 450-600 nm, it is possible to endow traditional red dye molecules with lasting luminescence by employing the PRET approach. As the fundamental requirements of Förster-type resonance energy transfer, the necessity for spectral overlap between the persistent luminescence emission band of the energy donor and the absorption band of the energy acceptor is crucial. Consequently, the commercially available fluorescent dye known as Rhodamine B (RB) was chosen as the energy acceptor, with the aim of attaining a broad spectrum of persistent afterglow that could be flexibly tuned in color (spanning from green to red). There is an obvious overlap between the absorption spectrum of RB and the RTP emission spectrum of the doped film BBI-Cl-M@PMMA (Fig. 2d), which suggests that employing RB as an energy acceptor to harvest the triplet energy from the energy donor BBI-Cl-M is viable. Indeed, a notable decline in the delayed emission intensity of BBI-Cl-M and a corresponding rise in that of RB are observed as the doping concentration of RB is progressively elevated from 30% to 150%.

The consistent alterations in the intensity of delayed emission suggest that PRET is taking place between the energy donor BBI-Cl-M and the energy acceptor RB. The RTP duration of BBI-Cl-M diminishes from 120.5 ms to 79.3 ms progressively, while the lifetime of the fluorescence emitted by RB extends from the nanosecond to the millisecond (Fig. 2g, Table S2 in Supporting information). Specifically, the color of the persistent afterglow can be progressively shifted from green to red as the concentration of RB doping is increased (Fig. 2h). In order to provide additional validation that the sustained delayed fluorescence in RB is initiated through PRET mechanism, the time-resolved emission spectra of the co-doped film RB/BBI-Cl-M@PMMA and the single-doped film RB@PMMA were obtained (Fig. 2e). Regarding the co-doped film RB/BBI-Cl-M@PMMA, the persistent fluorescence of RB is stimulated at the most suitable excitation wavelength for BBI-Cl-M (λ_{ex} =365 nm) rather than the most suitable excitation wavelength for RB (λ_{ex} =554 nm). Nonetheless, the doped film RB@PMMA, lacking the energy donor BBI-Cl-M, does not exhibit significant delayed fluorescence excited at 365 nm. Meanwhile, using the λ_{max} of RB's absorbance as excitation wavelength, persistent fluorescence also cannot be radiated for the acceptor RB (Fig. 2f). These above results reaffirm that the persistent triplet excitations of the energy donor BBI-Cl-M serve as the sole origin for imparting the fluorescent dye RB with enduring fluorescence properties through an effective PRET process. Additionally, as the doping weight concentration progressively rises from 30% to 150%, the lifetime of the energy donor decreases from 120.5 ms to 79.3 ms correspondingly. It is important to observe that the persistent fluorescence lifetime of RB still remains constant at ms (51.7 ms) even as its lifetime undergoes a progressive reduction (Fig. 2g), which also proves that the energy transfer goes smoothly.

To delve into the basic mechanisms of phosphorescence enhancement through polyatomic synergistic effects, single-crystal structural analysis was conducted, followed by a suite of computations using density functional theory (DFT) and time-dependent density functional theory (TD-DFT). These computations were designed to investigate the connection between the excited-state energy levels and the structural features. The mechanism of phosphorescence enhancement through polyatomic synergistic effects

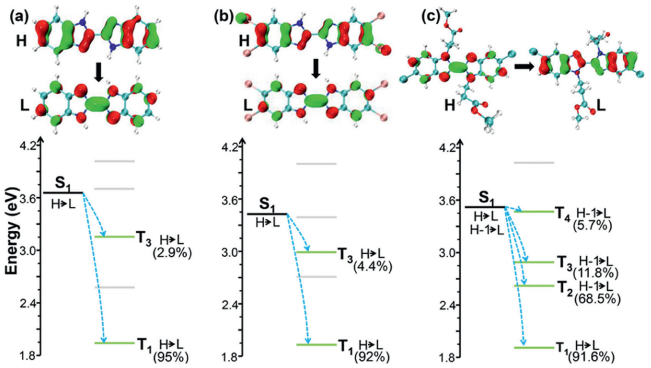

Fig. 3. HOMO and LUMO molecular orbital structures calculated by DFT, energy levels determined by TD-DFT, principal orbital configurations and potential ISC pathways (at the B3LYP/6-311G** computational level) for (a) BBI, (b) BBI-Br, (c) BBI-Cl-M. The S_1 represents the lowest singlet excited state, T_1 denotes the lowest triplet excited state and Tn refers to higher-level triplet excited states. The ISC channels that are likely to occur from the S_1 to the triplet states (T_n) are indicated with blue dashed arrows. More details were showed at Fig. S22 and Tables S5 and S6 (Supporting information).

is further elucidated through calculations using density functional theory and analysis of the single crystal structure. The triplet state T_2 energy levels of BBI, BBI-Br, BBI-Cl, BBI-M and BBI-Cl-M were calculated to be 2.8356 eV (437 nm), 2.7181 eV (456 nm), 2.7438 eV (452 nm), 2.7686 eV (448 nm) and 2.7538 eV (450 nm), respectively. The results align well with the detected ultralong phosphorescence bands, as evidenced in Fig. 3 and further confirmed by the entries in Tables S5 and S6.

Simultaneously, augmenting the spin-orbit coupling (SOC) matrix element that exists between the singlet and triplet states is likewise beneficial in boosting the intersystem conversion (ISC) rate, as shown by the equation:

$$k_{ISC} = \frac{2\pi}{\hbar}\left|\left\langle S\left|\hat{H}_{SOC}\right|T\right\rangle\right|^2\sqrt{\frac{\pi}{\lambda k_B T}}\exp\left[-\frac{\left(E_{ISC}-\lambda\right)^2}{4\lambda k_B T}\right] \quad (1)$$

In this expression, $\langle S|\hat{H}_{SOC}|T\rangle$ stands for the matrix element of spin-orbit coupling (SOC) between singlet and triplet states, $\hbar$ is the Planck constant, λ is the total reorganization energy, k_B is the Boltzmann constant, T is the temperature and E_{ISC} denotes the energy gap between the singlet state S_1 and a specific triplet state T_n [46,47]. BBI-Br and BBI-Cl exhibit significantly higher spin-orbit coupling values: BBI-Br ($\langle T_2|\hat{H}_{SOC}|S_0\rangle$ = 2.94 cm^{-1}, $\langle S_1|\hat{H}_{SOC}|T_3\rangle$ = 0.17 cm^{-1}) and BBI-Cl ($\langle T_2|\hat{H}_{SOC}|S_0\rangle$ = 0.41 cm^{-1}, $\langle S_1|\hat{H}_{SOC}|T_3\rangle$ = 0.03 cm^{-1}), compared to BBI ($\langle T_2|\hat{H}_{SOC}|S_0\rangle$ = 0.06 cm^{-1}, $\langle S_1|\hat{H}_{SOC}|T_3\rangle$ = 0.01 cm^{-1}) (Table S5 in Supporting information). This phenomenon can be ascribed to the influence of the heavy atom effect, which explains why BBI-Br and BBI-Cl exhibit strong and long-lasting phosphorescence dispersed in PMMA matrices.

Interestingly, BBI-Cl exhibits the strongest long-lasting phosphorescence among the three BBI derivations. In order to obtain more profound understanding of the reason behind superior phosphorescence capabilities of BBI-Cl, a single crystals X-ray analysis was conducted. Among these single crystal structures, C-X acts as a halogen bonding donor, C-H from benzene or π-electrons from imidazole serves as halogen bonding acceptor. As shown in Fig. 4, the distances of C-X$\cdots\pi$ in bibenzimidazole derivatives are 3.472 and 3.779 Å for BBI-Cl and BBI-Br, respectively. What's more, the distance for C-X$\cdots\pi$ halogen bonding of BBI-Cl is much shorter than BBI-Br, indicating much stronger intermolecular interactions in BBI-Cl (Fig. 4a, Tables S3 and S4 in Supporting information). Additionally, BBI-Cl is observed to possess a multitude of robust inter-

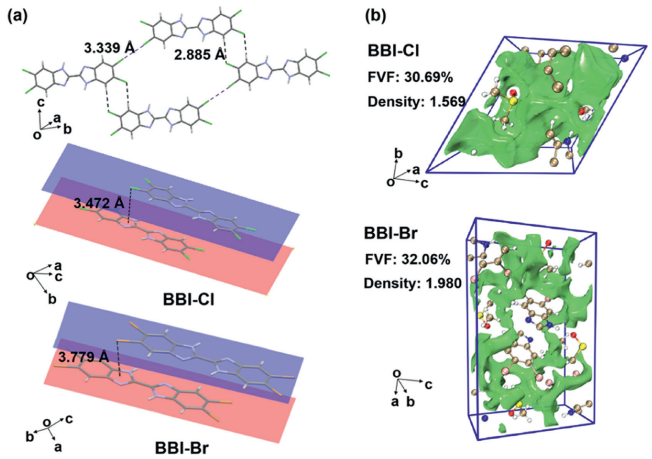

Fig. 4. Illustration of (a) the structures and intermolecular interactions in BBI-Cl, BBI-Br single crystal, (b) the FVFs obtained with Multiwfn 3.8 (dev) package.

molecular interactions, such as C-H···Cl-C and C-Cl···Cl-C. It is evident that the chlorine atom presented in BBI-Cl can establish robust interactions, effectively restricting molecular movements that lead to non-radiative transitions. This can also be explained as the reason for the optimal phosphorescent performance of BBI-Cl among three BBI derivatives. For BBI-Br single crystal, as a result of the decrease in intermolecular hydrogen bonding and the large size of bromine atoms, a loose packing is formed, furnishing a high free volume fraction (FVF) up to 32.06% (Fig. 4b). Therefore, choosing the appropriate atomic size and ensuring dense packing are two critical elements in reducing non-radiative to enhance ultralong RTP.

Since heavy atoms invariably lead to considerable energy dissipation [48], in the ester-modified bibenzimidazole derivatives, only one chlorine atom is introduced at the 5-position of each benzimidazole skeleton. Consistent with our predicted results, BBI-Cl-M displays the most pronounced phosphorescent properties (Fig. S16 in Supporting information). The theoretical calculations have also confirmed the results, as shown in Fig. 3 the configurations of the highest occupied molecular orbital (HOMO) and the lowest unoccupied molecular orbital (LUMO), along with the energy level diagrams for each of the three compounds, have been presented. Essentially, when the energy level of a triplet state (T_n) falls within the identical range as the energy level of the lowest excited singlet state (S_1) and shares identical transition orbital configurations (such as H→L and H-1→ L), the transition from S_1 to T_n constitutes a viable route for intersystem crossing (ISC). Taking these guidelines into account, for BBI, BBI-Br and BBI-Cl, there exist only two potential pathways for the transition from singlet to triplet states with the triplet state (T_n) possessing lower energy than the singlet state (S_1) and sharing the same transition configuration (H→L), which is not conducive to ISC. However, the introduction of ester groups resolved the issue of inadequate channels. Upon the integration of ester groups into the BBI-Cl-M system, four possible intersystem crossing (ISC) routes from the S_1 state to the triplet states T_1, T_2, T_3 and T_4 have been recognized. All these pathways involve transition configurations from the HOMO to the LUMO and from the HOMO-1 to the LUMO and the multiplication of ISC channels facilitates the ISC process, which in turn results in the strengthening of phosphorescence emission [49]. The coexistence of ester groups and chlorine atoms can generate a synergistic effect, which significantly enhances the phosphorescence performance of BBI-Cl-M. This synergy optimizes the molecular electronic structure, opens more intersystem crossing (ISC) channels and increases the efficiency of ISC. The intermolecular interactions between chlorine atoms and other atoms enhance the rigidity of the molecular structure, suppressing non-radiative transitions and thus promoting phosphorescence emission. The introduction of ester groups increases the polarity of the molecule and improves the interaction between molecular orbitals, which helps promote the release of energy through radiative transitions. Meanwhile, chlorine atoms increase the probability of the ISC process due to their so-called heavy atom effect, which facilitates the transition from singlet to triplet states. Our hypothesis is verified: these factors work together to give BBI-Cl-M more pronounced phosphorescent properties.

The development of UORTP materials with exhibit intense emission underwater has been a longstanding challenge in this field. As shown in Fig. 5a, PMMA can act as a perfect matrix, providing a rigid setting for the encapsulated molecules and protecting them from deactivation arisen from oxygen and water. Conversely, since for the high-level transparency of PMMA film, UV light can pass through its surface and trigger the encapsulated molecules. Once triggered, the confined molecules produce triplet excitons that initially use up the leftover oxygen within the film and the accumulation of triplet excitons begins subsequently. Then ultralong phosphorescence emerges and its intensity increases upon irradiation. Moreover, when the film is submerged in water, PMMA acts as a natural barrier preventing the re-entry of oxygen and the hydrophobic nature of PMMA also prevents water from entering the film, thereby the doped films underwater should exhibit superior phosphorescence performance compared to those exposed to air [35,50].

Considering its distinctive photo-activity and superior RTP performance, we showcased the practical applications of both the BBI-Cl-M@PMMA film and the RB/BBI-Cl-M@PMMA film. The size and form of the fabricated PMMA film can be readily adjusted to suit specific requirements. Firstly, the BBI-Cl-M@PMMA and RB/BBI-Cl-M@PMMA mixture is added into the mold. As the solvent gradually evaporates, the BBI-Cl-M@PMMA and RB/BBI-Cl-M@PMMA material exhibits excellent plasticity, enabling it to be easily shaped into various desired forms. To activate the samples, polymer materials are exposed to a portable ultraviolet lamp. As triggered by the UV irradiation, BBI-Cl-M@PMMA and RB/BBI-Cl-M@PMMA show vibrant and stable blue or red emission. Following the cessation of the excitation light, the phosphorescence lingers and shines for several seconds, highlighting the persistent and long-lasting nature of the emission (Fig. S23 in Supporting information). Additionally, this process demonstrates exceptional reproducibility. This reliability further enhances the practicality and applicability of the mold preparation strategy. As shown in Fig. 6a, the numeral "8" created from three distinct encoding materials provides a more intricate form of encryption. Once the UV light exposure is ceased, the shape of the numeral "8" gradually transforms into the numerals "9" and "7" in succession. Additionally, a beautiful cutout of bloomy rose is fabricated to enhance security measures. As depicted in Fig. 6b, exposed to UV light, the petals of the "rose" glow with an orange fluorescence, while the leaves emit a blue fluorescence. Interestingly the petals are turned into red afterglow and the leaves are turned into green afterglow when the UV light is ceased. With time elapsing, all the petals slowly disappear from view while the green leaves remain visible to the unaided eye.

In summary, a simple method was proposed to achieve persistent luminescence materials with ultralong lifetimes and broad color tunability through polyatomic synergistic effects and non-traditional PRET strategies. Specifically, by functionalizing BBI derivatives with ester groups and introducing modified chlorine atoms into molecular skeleton, a significant UORTP lifetime (τ_p) of up to 256.4 ms was realized. BBI-Cl-M, serving as the energy donor, was paired with traditional red-emitting dyes RB as the energy acceptor. The accomplishment of long-lasting multicolor or-

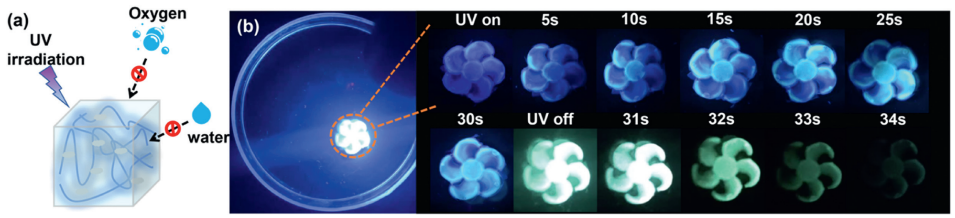

Fig. 5. (a) The possible mechanism of ultralong phosphorescence for doped PMMA films. (b) Luminescence photographs of the BBI-Cl-M@PMMA film submerged in water at various moments.

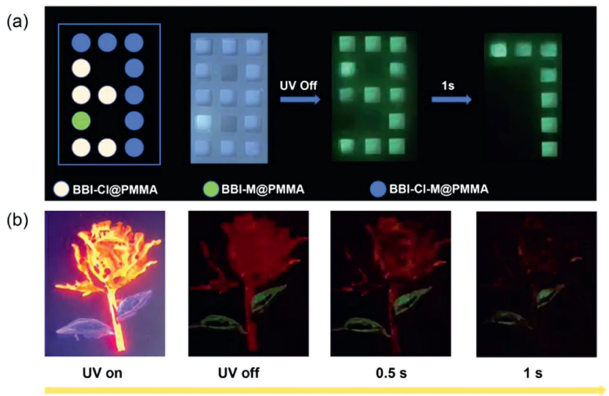

Fig. 6. Demonstration of multilevel anti-counterfeiting effects for RTP polymer materials.

ganic afterglow, spanning from the green to the red part of the spectrum, was efficiently realized by merely fine-tuning the doping ratios and concentrations within these unconventional PRET systems. Furthermore, it was discovered that BBI-Cl-M@PMMA films exhibit superior phosphorescent performance underwater compared to in air, offering a new perspective for applications such as underwater imaging. Various of multilevel encryption patterns were also explored, demonstrating the potential of BBI derivatives in underwater model making and advanced anti-counterfeiting fields. this new strategy based on polyatomic synergistic effects and PRET not only puts forward a potent method for preparing RTP materials with ultralong lifetime and broad color-tunability, but also paves the way for potential uses in complex ambient conditions.

Declaration of competing interest

The authors declare that they have no known competing financial interests or personal relationships that could have appeared to influence the work reported in this paper.

CRediT authorship contribution statement

Hong Yao: Writing – review & editing, Supervision, Conceptualization. **Feixiang Yang:** Writing – review & editing, Writing – original draft, Visualization, Methodology, Formal analysis, Data curation, Conceptualization. **Jianpeng Hu:** Writing – review & editing, Conceptualization. **Wenyu Cao:** Investigation. **Shuning Qin:** Investigation. **Tai-Bao Wei:** Writing – review & editing, Conceptualization. **Bingbing Shi:** Conceptualization. **Qi Lin:** Writing – review & editing, Writing – original draft, Resources, Conceptualization.

Acknowledgments

This work was supported by the National Natural Science Foundation of China (NSFC, Nos. 22061039, 22165027), the Top Leading Talents Project of Gansu Province, the Key R & D program of Gansu Province (No. 21YF5GA066), Gansu Province College Industry Support Plan Project (No. 2022CYZC-18) and Northwest Normal University 2023 graduate research funding project (No. 2023KYZZ-S154)

Supplementary materials

Supplementary material associated with this article can be found, in the online version, at doi:10.1016/j.cclet.2024.110375.

References

[1] X. Wang, G. Pan, H. Ren, et al., Angew. Chem. Int. Ed. 61 (2021) e202114264.
[2] Y. Yan, C. Liu, J. Fan, et al., Research 6 (2023) 0241.
[3] L. Huang, C. Qian, Z. Ma, Chem. Eur. J. 26 (2020) 11914–11930.
[4] G. Wang, Z. Wang, B. Ding, et al., Chin. Chem. Lett. 32 (2021) 3039–3042.
[5] Y. Wang, H. Gao, J. Yang, et al., Adv. Mater. 33 (2021) 2007811.
[6] X. Yao, J. Wang, D. Jiao, et al., Adv. Mater. 33 (2020) 2005973.
[7] D. Li, Y. Yang, J. Yang, et al., Nat. Commun. 13 (2022) 347.
[8] S. Cui, B. Wang, Y. Zan, et al., Chem. Eng. J. 431 (2022) 133373.
[9] Y. Wang, J. Yang, M. Fang, et al., Adv. Funct. Mater. 31 (2021) 2101719.
[10] J. Zhou, D. Liu, L. Li, et al., Chin. Chem. Lett. 35 (2024) 109929.
[11] T. Wang, Z. Hu, X. Nie, et al., Nat. Commun. 12 (2021) 1364.
[12] L. Bian, H. Shi, X. Wang, et al., J. Am. Chem. Soc. 140 (2018) 10734–10739.
[13] X. Wang, H. Shi, H. Ma, et al., Nat. Photonics 15 (2021) 187–192.
[14] J. Song, L. Ma, S. Sun, et al., Angew. Chem. Int. Ed. 61 (2022) e202206157.
[15] H. Li, H. Li, J. Gu, et al., Chem. Sci. 12 (2021) 3580–3586.
[16] H. Sun, L. Zhu, Aggregate 4 (2022) e253.
[17] H. Gao, X. Ma, Aggregate 2 (2021) e38.
[18] Y. Wang, C. Wang, J. Zhang, et al., Chin. Chem. Lett. 34 (2023) 108062.
[19] Y. Liu, G. Zhan, W. Liu, et al., Chin. Chem. Lett. 27 (2016) 1231–1240.
[20] Y. Sun, L. Jiang, Y. Chen, et al., Chin. Chem. Lett. 35 (2024) 108644.
[21] W. Zhao, Z. He, J.W.Y. Lam, et al., Chem 1 (2016) 592–602.
[22] J. Yang, X. Zhen, B. Wang, et al., Nat. Commun. 9 (2018) 840.
[23] O. Bolton, D. Lee, J. Jung, et al., Chem. Mater. 26 (2014) 6644–6649.
[24] Y. Gong, Y. Tan, J. Mei, et al., Sci. China Chem. 56 (2013) 1178–1182.
[25] C.R. Wang, Y.Y. Gong, W.Z. Yuan, et al., Chin. Chem. Lett. 27 (2016) 1184–1192.
[26] D. Lee, O. Bolton, B.C. Kim, et al., J. Am. Chem. Soc. 135 (2013) 6325–6329.
[27] T. Li, Y. Zheng, C. Wu, et al., Chin. Chem. Lett. 33 (2022) 4238–4242.
[28] J. Wang, Z. Huang, X. Ma, et al., Angew. Chem. Int. Ed. 59 (2020) 9928–9933.
[29] Z. An, C. Zheng, Y. Tao, et al., Nat. Mater. 14 (2015) 685–690.
[30] C.C. Zhang, S. Yuan, Y.H. Lou, et al., Adv. Mater. 32 (2020) 2001479.
[31] X. Zheng, J. Jiang, Q. Lin, et al., Chem. Eng. J. 469 (2023) 143929.
[32] K. Zhang, L.Y. Peng, X.X. Liu, et al., Angew. Chem. Int. Ed. 62 (2023) e202300927.
[33] S. Li, Z.Y. Zhang, J.F. Lv, et al., J. Mater. Chem. A 11 (2023) 4957–4962.
[34] H. Shi, Z. An, P.Z. Li, et al., Cryst. Growth Des. 16 (2016) 808–813.
[35] S. Xiong, Y. Xiong, D. Wang, et al., Adv. Mater. 35 (2023) e2301874.
[36] N. Gan, X. Zou, M. Dong, et al., Nat. Commun. 13 (2022) 3995.
[37] Q. Dang, Y. Jiang, J. Wang, et al., Adv. Mater. 32 (2020) e2006752.
[38] S. Kuila, S.J. George, Angew. Chem. Int. Ed. 59 (2020) 9393–9397.
[39] L. Kong, Y. Zhu, S. Sun, et al., Chem. Eng. J. 469 (2023) 143931.
[40] Y. Zhu, S. Sun, H. Li, et al., Eur. Polym. J. 202 (2024) 112600.
[41] L. Kong, S. Sun, Y. Zhu, et al., Dyes Pigm. 226 (2024) 112131.
[42] Y.Q. Zhu, X.H. Wang, M.X. Wu, Adv. Funct. Mater. 33 (2023) 2308096.
[43] S. Sun, J. Wang, L. Ma, et al., Angew. Chem. Int. Ed. 60 (2021) 18557–18560.
[44] G. Jiang, Q. Li, A. Lv, et al., J. Mater. Chem. C 10 (2022) 13797–13804.
[45] T. Zhang, X. Ma, H. Tian, Chem. Sci. 11 (2020) 482–487.
[46] H. Zhu, I. Badia-Dominguez, B. Shi, et al., J. Am. Chem. Soc. 143 (2021) 2164–2169.
[47] W. Zhao, Z. He, B.Z. Tang, Nat. Rev. Mater. 5 (2020) 869–885.
[48] X. Yang, S. Wang, K. Sun, et al., Angew. Chem. Int. Ed. 62 (2023) e202306475.
[49] D. Beljonne, Z. Shuai, G. Pourtois, et al., J. Phys. Chem. A 105 (2001) 3899–3907.
[50] C. Qian, X. Zhang, Z. Ma, et al., CCS Chem. 6 (2024) 798–811.